Tube Extrusion of Polymeric Materials: Optimization of the Processing Parameters

A. G. Mamalis,[1] A. K. Vortselas,[2] G. Kouzilos[2]

[1]*Project Center for Nanotechnology and Advanced Engineering, National Center of Scientific Research "Demokritos," Athens, Greece*
[2]*Laboratory of Manufacturing Technology, National Technical University of Athens, Athens, Greece*

Received 8 September 2011; accepted 27 November 2011
DOI 10.1002/app.36555
Published online in Wiley Online Library (wileyonlinelibrary.com).

ABSTRACT: In the study described in this article, we aimed to apply multiparametric optimization to the processing conditions in a spider die used for the extrusion of polymers, in this case, high-density polyethylene tubes. Product quality is affected by the homogeneity of the flow speed and the temperature at the die exit. Inhomogeneity causes shape distortions and material weak spots (weld lines), and its major cause in spider dies is the discontinuity and distortion of the flow caused by *spider legs*, the ties by which the inner mandrel of the die is secured to its external casing. The Nelder–Mead nonlinear optimization technique was applied to the numerical model to pinpoint the processing conditions, namely, the inlet pressure, inlet temperature of the melt, temperature of the die walls, and temperature of the spider legs.
 J Appl Polym Sci 000: 000–000, 2012

Key words: computer modeling; extrusion; polyethylene (PE)

INTRODUCTION

A common manufacturing process for plastic tubes and other components with a closed cross section is the extrusion of polymeric materials with an annular inline or straight-through die. In such processes, product quality is affected by the homogeneity of the flow speed and temperature at the die exit. Inhomogeneity causes shape distortions and material weak spots (weld lines). The major cause for such inhomogeneity in spider dies is the discontinuity and distortion of the flow caused by the *spider legs*, the ties by which the inner mandrel of the die is secured to its external casing, whereas the die sections aft of the spider work to rehomogenize the flow. In this study, we aimed to apply multiparametric optimization to the processing conditions in a spider die used for the extrusion of polymers, in this case, high-density polyethylene (HDPE) tubes.

For this purpose, a computational fluid dynamics (CFD) based model using the generalized Newtonian approach was employed to investigate the pressure drop, along with the flow and temperature uniformity in the die (Fig. 1). CFD-based approaches were developed previously by other researchers to study various aspects of flow in extrusion dies.[1–5] The numerical calculations of the three-dimensional flow and temperature fields were performed with a finite-element-based CFD code, Comsol 3.5 (COMSOL AB, Stockholm, Sweden).

The Nelder–Mead nonlinear optimization technique was applied to the numerical model to pinpoint the processing conditions that result in the maximization of flow homogeneity at the die outlet and consequently achieve the best product quality. The parameters investigated were inlet pressure (p_{in}), inlet temperature of the melt (T_{in}), temperature of the die walls (T_h), and temperature of the spider legs (T_f). During extrusion, the pressure was determined by the control of the motor of the extruder screw, whereas the temperatures were controlled in each section via independent heating elements.

The objective function used was a weighted average of the signal-to-noise ratio (SNR) values of the flow temperature and velocity at the die outlet. The SNRs were taken as a measure of the residual disturbance that the existence of the spider legs caused to the flow homogeneity in the azimuthal direction.

NUMERICAL MODEL AND OPTIMIZATION METHODS

The geometry of the modeled flow tube was derived as shown in Figure 2. The spider die design was assembled in a three-dimensional computer-assisted design environment. The die in question produced a tube with a 32-mm outside diameter and a 2.4-mm wall thickness. The fluid volume was extracted from the die assembly, and one-twelfth of it (we took

Correspondence to: A. G. Mamalis (mamalis@ims.demokritos.gr).

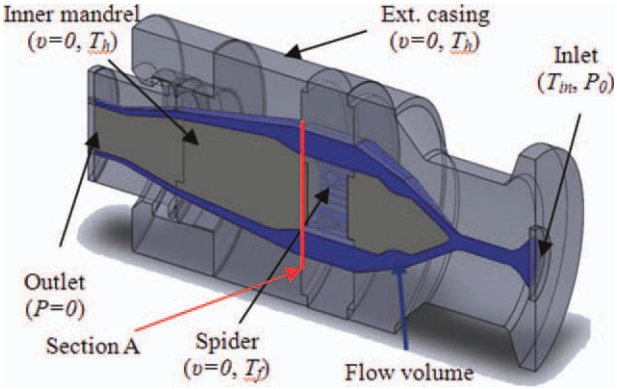

Figure 1 Sectional view of the assembly of the spider die and melt volume and boundary conditions of melt flow υ, pressure P and temperature T. [Color figure can be viewed in the online issue, which is available at wileyonlinelibrary.com.]

advantage of symmetry planes) was imported in the finite element method environment, where the volume was meshed and the problem was solved. Postprocessing of the solution involved the sampling of the velocity and temperature at various cross sections of the die.[6]

Carreau–Yasuda model

Because the material properties greatly affect the analysis of the entire processing operation, the use of reliable models is essential. However, in many polymer processes, the elastic memory effects are not very important because the melts are subjected to large steady rates of deformation for a relatively long period of time.[7] Because this study was concentrated on a qualitative analysis of the flow regimes, the inelastic model was selected. Polymer melts are non-Newtonian fluids. The viscosity–shear rate dependence of non-Newtonian liquids is typically represented by one of several viscosity models and is referred to as the *viscosity*.[8] Various models exist for describing the dependence of the viscosity on the shear rate and temperature. A great deal of flexibility is provided by the Carreau–Yasuda model:

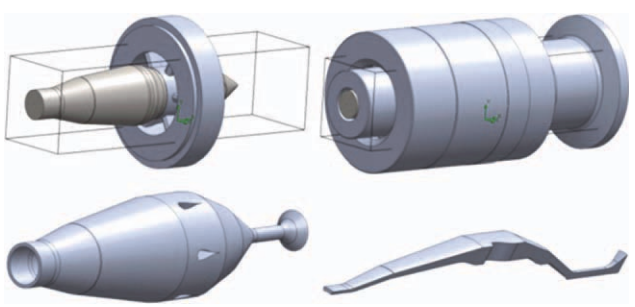

Figure 2 Derivation of the simulated flow volume. [Color figure can be viewed in the online issue, which is available at wileyonlinelibrary.com.]

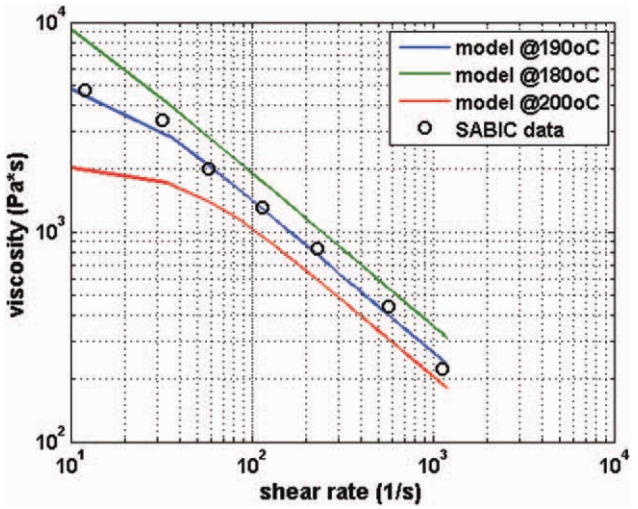

Figure 3 Recorded by the manufacturer (SABIC) viscosities of HDPE at 180, 190, and 200°C and their fits according to the Carreau–Yasuda and power law models. [Color figure can be viewed in the online issue, which is available at wileyonlinelibrary.com.]

$$\eta = a_T \eta_0(T_R)\left[1 + \left(a_T \dot{\lambda}(T_R)\dot{\gamma}\right)^a\right]^{(n-1)/a} \quad (1)$$

where the shift factor (a_T) is defined as

$$a_T = \exp[E_0/R(1/T - 1/T_R)] \quad (2)$$

where η_0, λ, a, and n are the fitting parameters and TR is the reference temperature. More specifically, η_0 is the viscosity at a shear rate of zero, λ is the time constant, with its reciprocal representing the shear rate at the transition from Newtonian to shear-thinning behavior, a determines the width of the transition region, and n is the power law index that describes the slope of the viscosity curve with respect to the shear rate in the shear-thinning region. The temperature dependence in the Carreau–Yasuda model is introduced in eq. (2) through a_T, where E_0 is the activation energy and R is the universal gas constant. The shear viscosity and shear rate dependence of the polymer is presented in Figure 3. The parameters used in the Carreau–Yasuda model are given in Table I.

The temperature dependence of the physical properties of HDPE are given in Table II as polynomials of the form $A + BT$, where T is the temperature (°C).[9]

TABLE I
Carreau Model Constants

Model parameter	
n	0.2723
η_0	5.43×10^3 Pa s
λ	0.063 s
E_0	6.5 kcal/mol
T_R	190°C
A	2

TABLE II
Temperature Dependence of the Physical Properties of HDPE

Physical property	Polymer type	Temperature (°C)	*A*	*B*
k (W m^{-1} K^{-1})	HDPE	143–200	0.26	—
C_p (kJ kg^{-1} K^{-1})	HDPE	133–200	1.984	3.88×10^{-3}
ρ^{-1} (cm^3/g)	HDPE	133–200	1.158	8.09×10^{-4}

k: thermal conductivity; Cp: specific heat capacity; ρ-1: specific volume

Finally, an incompressible steady-state laminar flow is assumed, and sticking conditions are assumed for the die walls. The melt undergoes viscous dissipation (frictional heating), so the problem is fully coupled.

Objective function

Our optimization problem consisted of determining an geometry optimal for homogenizing the velocity distribution through the die exit that corresponded to the minimum of the velocity dispersion. The inhomogeneity of the flow velocity distribution is often addressed as the variability in a velocity measurement experiment. The variability of a property is due to the noise factor, which is difficult to control, and can be expressed by the SNR, measured in decibels. Hence, the SNR for flow velocity at the nodes of the melt exit cross section was chosen as the objective function for homogeneity (the maximum was better):

$$\mathrm{SNR} = 10 \log_{10} \left(\frac{\bar{X}^b}{s} \right)^2 \tag{3}$$

where $\overline{X}$ and s are the mean and standard deviation of the velocity or temperature and the exponent b is derived from the least-squares regression over the observed data: $\log_{10} s_i = a + b \times \log_{10} \overline{X}_i$. In our case, $b = 1$, with a very high R value.

Multiparametric objective function

After the two signal-to-noise values were obtained for the velocity and temperature (SNR_U and SNR_T, respectively), an objective function had to be constructed, to be minimized by the optimization. We used two such functions:

$$I_1 = -\left(w_1 \frac{\mathrm{SNR}_U}{\mathrm{SRN}_{U0}} + w_2 \frac{\mathrm{SNR}_T}{\mathrm{SRN}_{T0}} \right) \tag{4}$$

$$I_2 = \frac{w_1}{\mathrm{SNR}_U} + \frac{w_2}{\mathrm{SNR}_T} \tag{5}$$

where I_1 is a weighted function of the SNRs relative to an initial, reference condition so that the velocity and temperature can be treated equivalently and I_2 is a weighted function of the SNRs, which takes into account that one parameter may already be more homogeneous than the other.

Constraints

The problem was optimized inside a zone considered safe by empirical rules: $p_{\mathrm{in}} = 100$–250 bar at all temperatures (443–473 K, 170–200°C).

Nelder–Mead nonlinear optimization

Our optimization problem was nonlinear, and the objective function could have had multiple local minima. Stochastic optimization methods, such as genetic algorithms, simulated annealing, swarm methods, and artificial neural networks, have been used for such problems, even in forming, extrusion, and die design problems.[10,11] However, when each iteration consists of a computationally heavy numerical simulation, the slow convergence of such methods renders them impractical. In such cases, nonlinear gradient methods are much more economical, even though multiple repetitions from various initial points may be required to ensure the discovery of a global minimum. The Nelder–Mead method is such a technique and was successfully employed in similar problems by Tumer and Sonmez.[12] Details about this algorithm can be found in Lagarias et al.[13]

Nonparametric optimization (Pareto front)

To accomplish a meaningful multiparametric optimization, we had to be able to select the weights in a definitive fashion. Empirical knowledge about product quality from industry sources suggested a choice of weights: $w_1 = 0.8/w_2 = 0.2$. It would be much more useful, however, to be able to quantify the tradeoffs that had to be made when the weights were selected and how the optimum points would shift in relation to that.

To this effect, with the simulated experimental points that were accumulated with multiple runs of the Nelder–Mead algorithm, the Pareto front was extracted for each case. The Pareto front is the locus of experimental points that may be found to be optimal under some choice of weights, whereas the points not of the front would never be optimal, no matter the choice of points; related theory is presented in Kim and de Weck.[14] An optimization that converges not to a single point but to the entire Pareto front is thus called *nonparametric.* This technique has been used in similar problems.[15–17] A good approximation of the Pareto front may be the basis for the application of a stochastic optimization algorithm. It should be noted that a Nelder–Mead optimization should always converge to a point on the Pareto front, and when it does not, its convergence should be considered incomplete.

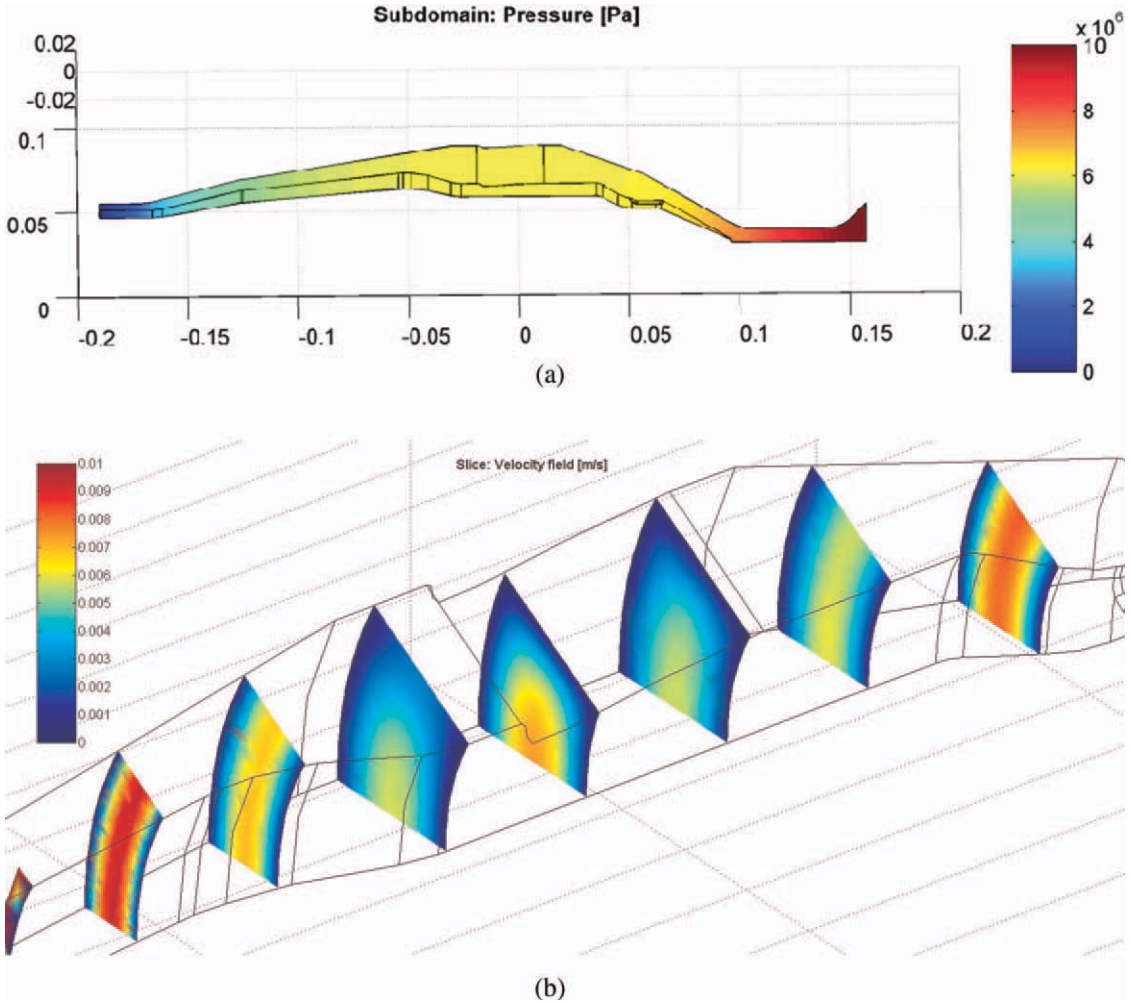

Figure 4 (a) Pressure and (b) velocity distributions. [Color figure can be viewed in the online issue, which is available at wileyonlinelibrary.com.]

RESULTS AND DISCUSSION

Figure 4(a) shows the pressure distributions in the entire domain of the die, as calculated by one of the finite element simulations. The pressure decreased continuously from die inlet to the outlet, and the melt flow rate was a monotonous function of it. The axial thrust load on the die core was 3.04–3.36 kN. The viscosity dropped at high-velocity zones but remained above 5000 Pa s in the spider section. The flow was decelerated at the spider zone because of the higher cross section; then, it was accelerated and homogenized in the relaxation and end zones [Fig. 4(b)]. The calculated increase in the melt temperature due to viscous dissipation was only about 2 K.

In an examination of the cross sections of the melt velocity and temperature (Fig. 5), the boundary effect of the die walls and the effect of the spider leg, which reduced velocity and altered the melt temperature, were revealed. To calculate the homogeneity, these cross sections could be sampled either uniformly on their whole surface or over an azimuthal arc at their mean radius. For precision-related reasons, the latter was the preferred method.

Mesh convergence

To ensure a valid and stable optimization, we had to ascertained that numerical noise, which is inserted into the problem by the discrete nature of the finite element mesh, did not affect the SNR values extracted (see also Lebaal et al.[10]). To that effect, a convergence check was performed for the parameters that controlled the mesh density, namely:

- General mesh density (h_{auto}; Fig. 6).
- Maximum element size (h_{max3}; spider).
- Maximum element size (h_{max4}; die sections 4 and 5).
- Maximum element size (h_{max5}; die outlet).

The convergence test was applied to reference conditions ($p_{in} = 100$bar, $T_{in} = T_h = T_f = 469$ K). As shown in Figure 7, for both velocity and temperature

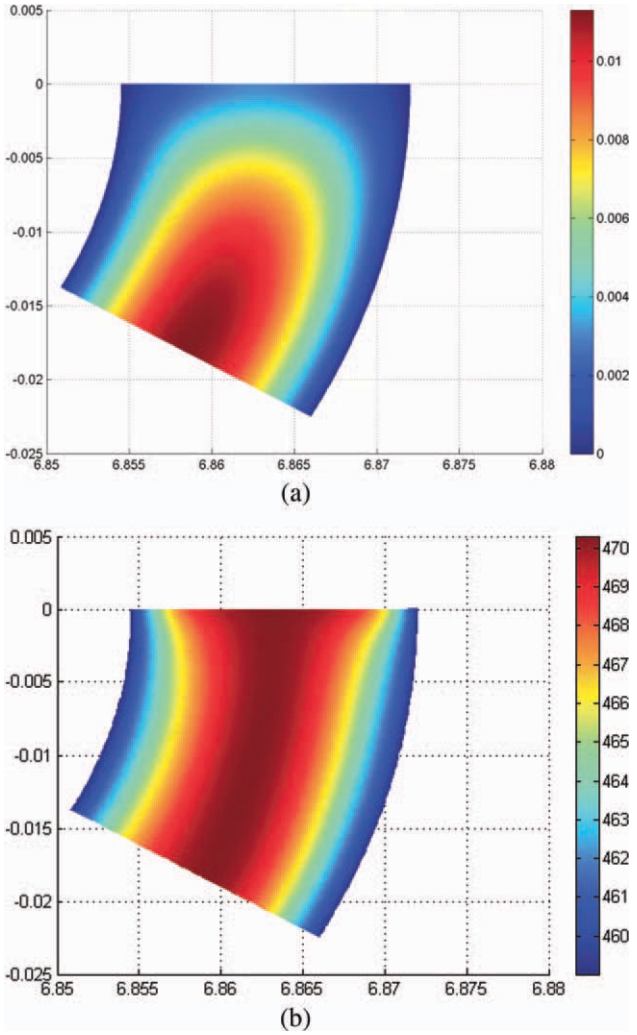

Figure 5 (a) Melt velocity and (b) temperature of the cross sections just aft of the spider. The upper edge was aligned behind a spider leg. [Color figure can be viewed in the online issue, which is available at wileyonlinelibrary.com.]

with either surface or azimuthal sampling, the SNRs for standard mesh quality varied by about 5% around those for best quality. The variance of the SNR values from these results had to be compared to the variance found among the results of the optimization experiment. The results of the optimization experiments had variances of 0.5% for velocity and 0.4% for temperature for the SNRs with surface sampling, whereas in the azimuthal case, these were 8.7 and 3.6%, respectively. When we sampled just aft of the spider, the experiment variances became 8 and 0.6%, respectively, for surface sampling and 8 and 2.2%, respectively, for azimuthal sampling.

The comparison enhanced the argument that the optimization parameters had to be sampled azimuthally and preferably also at a cross section forward of the die exit to provide meaningful results. It also provided the tolerance level for the convergence of the optimization algorithm. We also observed that the overall mesh quality did not affect the average SNR levels, but the cross-sectional mesh density significantly increased them. Thus, it was a parameter that had to be strictly controlled to obtain comparable results.

Nelder–Mead optimization

Case I: Results for section A

On the basis of the previous observations, the optimization algorithm was employed for the four parameters depicted in Figure 1. The optimization was performed for a cross section of the flow just aft of the spider with function I_1 [eq. (4)] for a set of five different weights (Fig. 8 and Table III).

It was evident that convergence was dominated by SNR_T. Because of this, p_{in} converged at various local minima close to the initial point. More interesting was the convergence of the temperatures: T_h and T_f converged together, which was somewhat

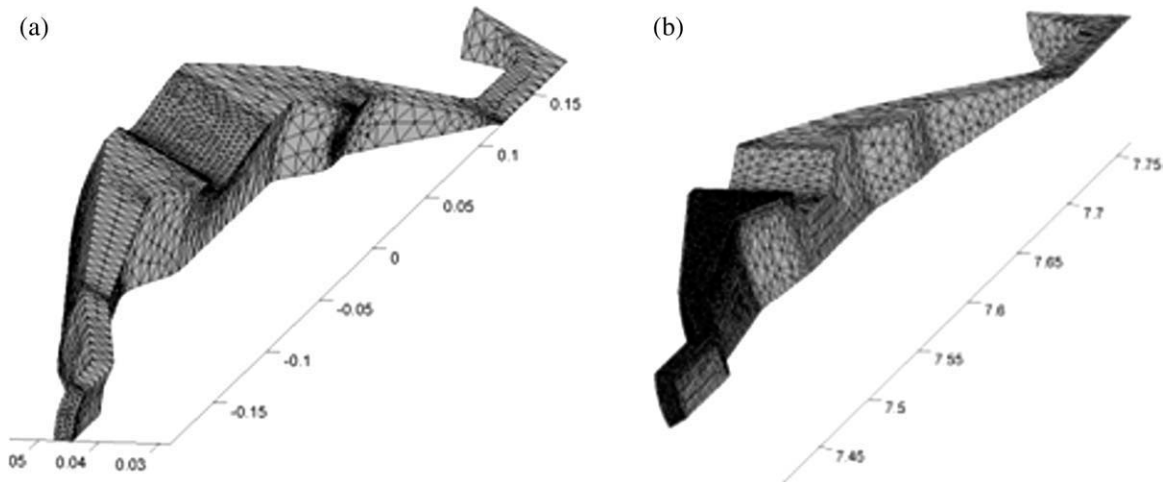

Figure 6 Mesh construction for different densities.

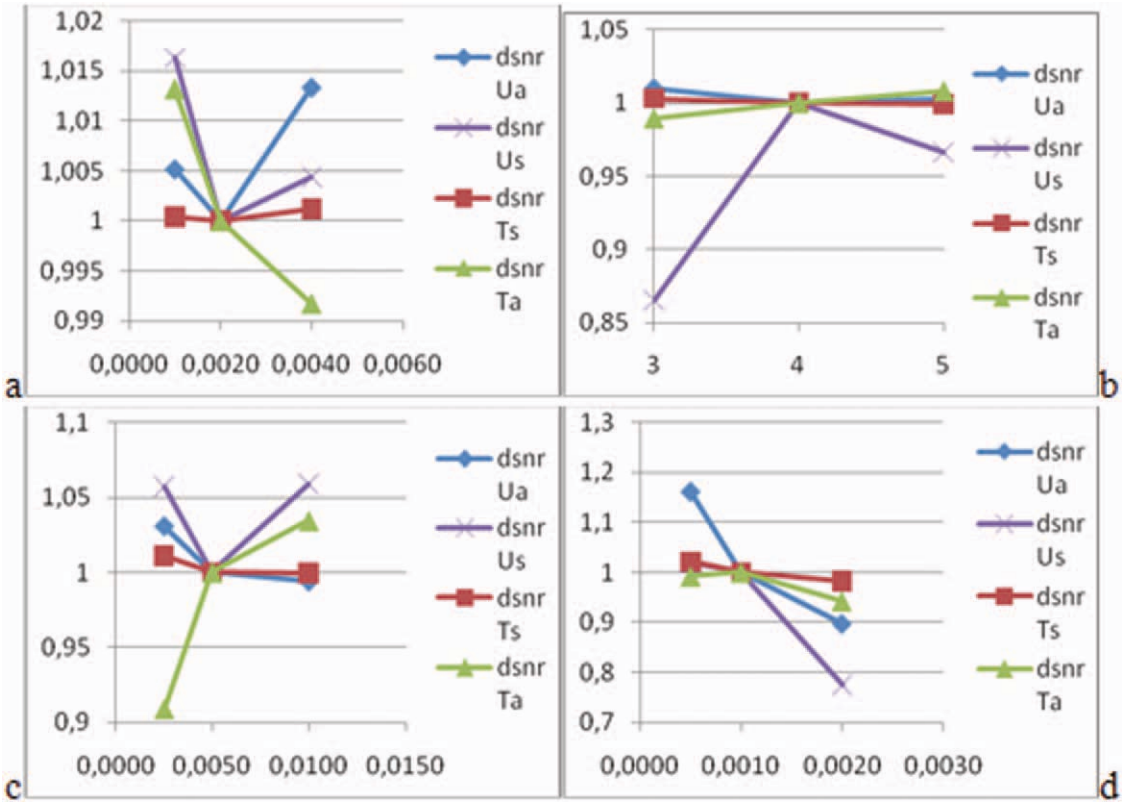

Figure 7 Relative effect of various mesh parameters on the SNRs of velocity (U) and temperature (T) with surface (s) and azimuthal (a) sampling: (a) h_{auto}, (b) h_{max3}, (c) h_{max4}, and (d) h_{max5}. [Color figure can be viewed in the online issue, which is available at wileyonlinelibrary.com.]

expected, whereas T_{in} converged to 1–1.5° below them; this was consistent with the observed difference attributed to viscous shearing.

Evaluation case studies: Case II

Using function I_2 [eq. (5)] and setting the weights to 80–20, we performed some testing to establish the effects of the different functions and initial points on the optimum obtained. As before, p_{in} converged at various local minima close to the initial point; the temperatures converged with great differences between them: $T_h - T_{in} = 8$–9 K. T_f went to a maximum (473 K).

Case III: Results for the outlet section

Using function I_2 and sampling at the die outlet instead of section A, we optimized the flow for a set

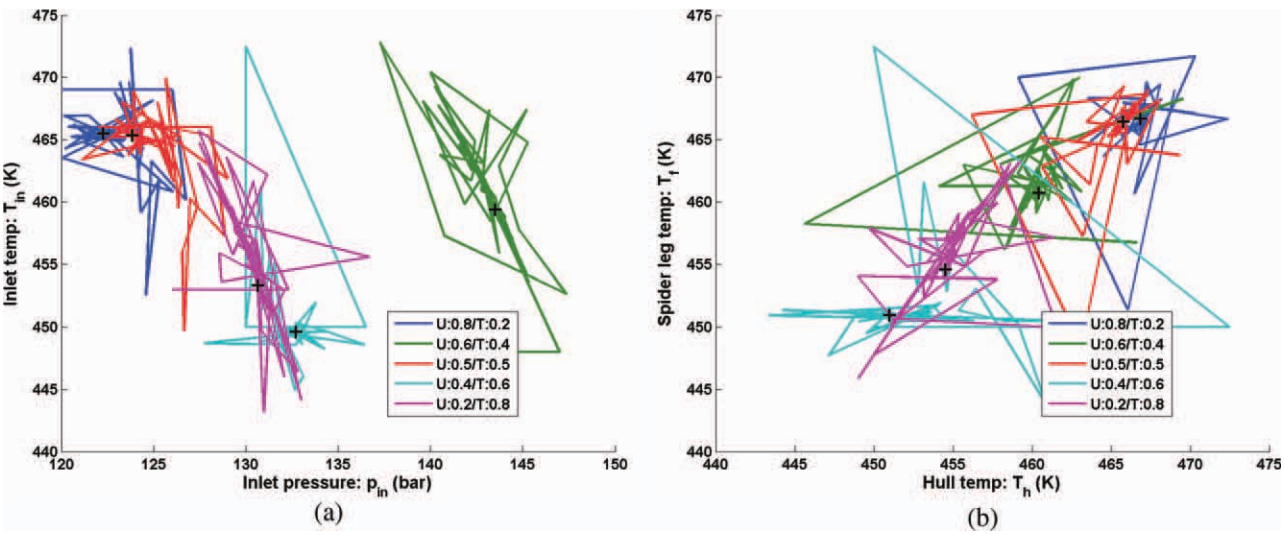

Figure 8 Paths of the optimization algorithm in variable space for (a) p_{in} and T_{in} and (b) T_h and T_f. [Color figure can be viewed in the online issue, which is available at wileyonlinelibrary.com.]

TABLE III
Optimum Points for Various Weights of the Objective Function

Weights w_1/w_2	p_{in} (bar)	T_{in} (K)	T_h (K)	T_f (K)
80–20	122.3	465.5	466.9	466.7
60–40	143.5	459.4	460.4	460.7
50–50	123.9	465.3	465.8	466.4
40–60	132.7	449.6	451.0	450.9
20–80	130.7	453.3	454.5	454.6

of three different weights. The new cross section had, of course, much greater SNRs, which were not comparable to those previously computed and which were also affected by mesh-induced errors. The pressure now had a catalytic effect, so p_{in} converged to a minimum (100 bar), T_h and T_{in} converged to 462–467 K, depending on the weights, and $T_f - T_h = 3.4$–5.7 K.

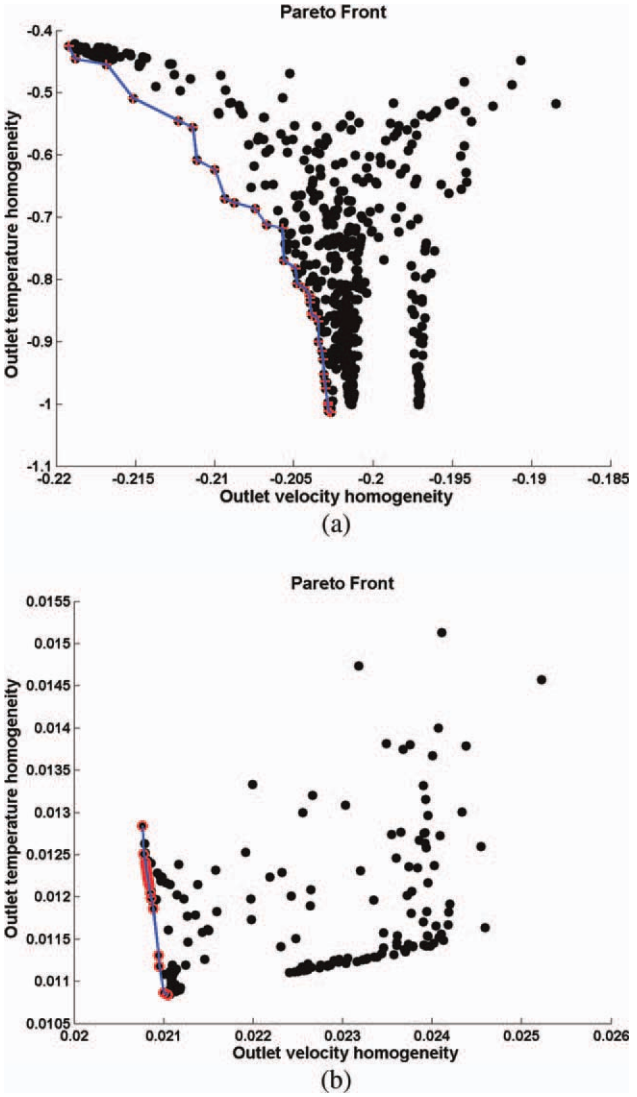

Figure 9 Determination of the Pareto front for cases (a) I and (b) III. [Color figure can be viewed in the online issue, which is available at wileyonlinelibrary.com.]

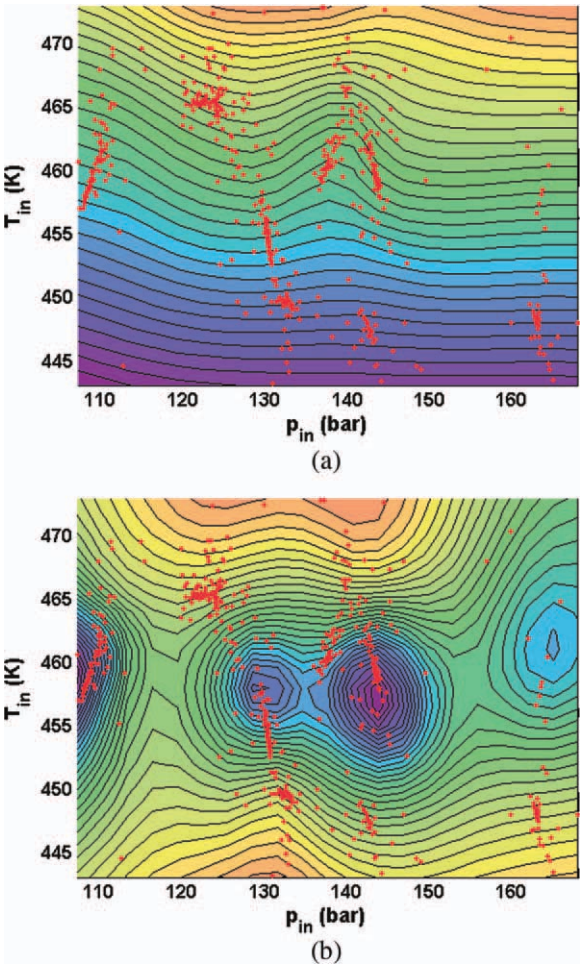

Figure 10 Mapping of (a) hom_U and (b) hom_T versus p_{in} and T_{in} for $T_h = T_f = 458$ K [The simulation points are shown as dots (red dots in the color figure online).] [Color figure can be viewed in the online issue, which is available at wileyonlinelibrary.com.]

Pareto front

The determination of the Pareto front was based on the exploitation of all available simulation points after the removal of any duplicates. For cases I and II, the front roughly followed a rational function [in absolute values; Fig. 9(a)]:

$$\text{hom}_T \approx \frac{0.28\text{hom}_U - 0.050}{\text{hom}_U - 0.197} \tag{6}$$

hom_U, hom_T are the homogeneities of velocity and temperature respectively, as defined in Eqs. (4), (5). For case III, the Pareto front was now linear [Fig. 9(b)]:

$$\text{hom}_T \approx -6.936\text{hom}_U + 0.1567 \tag{7}$$

Mapping of the homogeneities

The homogeneities over variable space were mapped on the basis of the available experimental points

with a radial basis function interpolation, with cubic support, as introduced by Baxter.[18] This way, out of 307 points, gridded maps for SNR_U and SNR_T, consisting of $21^4 = 194{,}481$ points, were constructed. In Figure 10, two-dimensional sections of those maps are displayed. The mapping accuracy was greater where the simulation points are concentrated.

The mapping demonstrated the gradients present during optimization, albeit in a limited way because of the reduction from four to two dimensions. The difficulty that arose for the convergence of p_{in} is evident.

CONCLUSIONS

In summary, the main features of our results are as follows:

- A non-Newtonian CFD model of the spider die polymer extrusion process was used as the input for a nonlinear multiparametric optimization process to determine the optimal processing conditions for achieving a homogeneous tube product.
- This analysis revealed that to achieve a homogeneous flow velocity, we had to trade off a significant amount of temperature homogeneity. This was true regardless of the weights we assigned to reflect the importance of the two parameters of product quality. It was also true regardless of the way we formulated the objective function or the choice of the cross section to be sampled.
- Contrary to conventional knowledge, the p_{in}/melt flow rate couple did not drastically affect homogeneity inside the search area of the optimization. Obviously, the pressure was already within the optimal range; thus, the variation of outputs was too small. The temperatures did, on the other hand, need to be controlled with precision for optimal results.
- The methods discussed provided valuable insight into the very difficult task of controlling the processing parameters for optimum product quality. They are generalizable for all extrusion processes of either polymers or metals and for any extruded shape.

References

1. Sun, Y.; Gupta, M. Soc Plast Eng Annu Tech Conf Tech Pap 2004, 3307.
2. Michaeli, W.; Kaul, S. J Polym Eng 2004, 24, 123.
3. Ettinger, H. J.; Sienz, J.; Pittman, J. F. T.; Polynkin, A. Struct Multidisc Optim 2004, 28, 180.
4. Zhang, M.; Sun, S.; Jia, Y. Polym–Plast Technol Eng 2008, 47, 384.
5. Mamalis, A. G.; Spentzas, K. N.; Kouzilos, G.; Theodorakopoulos, I.; Pantelelis, N. G. J Adv Polym Technol 2010, 29, 173.
6. Mamalis, A. G.; Kouzilos, G.; Vortselas, A. K. J Appl Polymer Science 2011, 122, 3537.
7. Michaeli, W. Extrusion Dies for Plastics and Rubber; Hanser: Munich, 1992.
8. Macosko, C. W. Rheology: Principles, Measurements, and Applications; Wiley-VCH: New York, 1994.
9. Baird, D.; Collias, D. Polymer Processing—Principles and Design; Wiley: New York, 1998.
10. Lebaal, N.; Puissant, S.; Schmidt, F. M. J Mater Proc Tech 2005, 34, 1524.
11. Pujos, C.; Regnier, N.; Defaye, G. Chem Eng Process 2008, 47, 456.
12. Tumer, H.; Sonmez, F. J Mater Proc Tech 2009, 209, 1538.
13. Lagarias, J. C.; Reeds, J. A.; Wright, M. H.; Wright, P. E., 1998. SIAM J Optim 1998, 9, 112.
14. Kim, I. Y.; de Weck, O. L. Struct Multidisc Optim 2005, 29, 149.
15. Soury, E.; Behravesh, A. H.; Rouhani Esfahani, E.; Zolfaghari, A. Mater Des 2009, 30, 4183.
16. Wei, L.; Yang, Y. J Mater Proc Tech 2008, 208, 499.
17. Sun, G.; Li, G.; Gong, Z.; Cui, X.; Yang, X.; Li, Q. Mater Des 2010, 31, 1917.
18. Baxter, B. J. C. Ph.D. Thesis, Cambridge University, 1992.